Lateral Torsional Buckling of Cellular Steel Beams

J. Nseir[1], M. Lo[2], D. Sonck[3], H. Somja[2], O. Vassart[4], N. Boissonnade[1]

Abstract

Present paper deals with the behavior of so-called cellular members against lateral torsional buckling. These beams comprising regularly-spaced web openings are especially used for their high resistance-weight ratio, the possibility to integrate service pipes within their height, and aesthetics. Such profiles usually exhibit a complex behavior, since they can experience many modes of failure, including local instability ones, i.e. those involving an out-of-plane instability of the web post at high shear locations and/or distortion of the cross-section.

For what regards global instability, the members are usually designed by means of rough design rules, which often lead to an unduly conservative girder, the beams sometimes showing over 200% resistance reserve. Present research aims at improving this situation, by means of new adequate design formulae.

In this respect, both experimental and extensive numerical parametric studies have been undertaken. First, a series of 3 full-scale tests has been performed, the main goal of which being the validation of purposely-derived FE models. Since the numerical models showed a very good agreement with the tests, they have been further used to gather a large set of numerical reference results where many parameters were varied: the relative slenderness, steel grades, cross-section shapes, bending moment distributions, and relative sizes of the openings. Finally, a new set of dedicated design rules has been derived, that was proved to be accurate while leading to safe estimates of the resistance when compared to all reference results.

1. Motivation – Scope of research investigations

Present paper deals with the behavior of so-called "cellular members" submitted to major-axis bending, with a specific focus on their Lateral Torsional Buckling resistance (LTB). Such girders beams are usually manufactured through a specific industrial process, by means of flame-cutting the web of an existing H or I-shaped hot-rolled profile along a specific path (see Fig. 1a), then welding the separated "Tees" tip-to-tip together, see Fig. 1c.

---

[1] University of Applied Sciences of Western Switzerland, <joanna.nseir@edu.hefr.ch>,
<nicolas.boissonnade@hefr.ch>
[2] National Institute of Applied Sciences of Rennes, <moussa.lo@insa-rennes.fr>, <hugues.somja@insa-rennes.fr>
[3] Ghent University, <delphine.sonck@ugent.be>
[4] ArcelorMittal Commercial Sections, <olivier.vassart@arcelormittal.com>

Figure 1: Fabrication process a) Principle – b) Flame cutting – c) Welding of webs

The additional costs generated by these operations are usually more than compensated by the increase in resistance and moment of inertia of the final girder, provided a minimum length of the member; typically, floor solutions involving 12 m and above spans may be found to be more economical through the use of such cellular beams.

Further to significantly increasing the inertia-to-weight ratio, they provide efficient solutions to the incorporation of building services within the structural depth of the floor (Fig. 2).

Figure 2: Use and advantages of cellular members

Such profiles usually exhibit a complex behavior, since they can experience many modes of failure (cf. Kerdal 1984), including local instability ones, i.e. those involving an out-of-plane instability of the web-post at high shear locations and/or distortion of the cross-section. For what concerns *global* instability (i.e. member instability, LTB), one may point out that their sensitivity to LTB is higher than that of their base profile, since the final height is usually much more important. As a consequence, the sections of cellular members, seen as a whole, are more slender, thus more prone to LTB.

Besides this, the resistance of cellular beams to LTB is also significantly affected by the presence of the openings: the LTB resistance of a cellular member may indeed theoretically vary from the LTB resistance of a usual I-shaped profile (i.e. with no openings) to that of a "Tee-section" column in weak axis buckling, corresponding to the lateral buckling of the "flange + part of web" in compression (situation with very large openings). Consequently, the carrying capacity of the girder can vary in a rather large extent between these two extreme cases.

The problem of LTB in cellular members therefore deserves specific attention and adequate treatment; it shall perhaps be pointed out that, in practical situations, the resistance to LTB is often the governing criterion in the erection phase of a composite beam. However, it appears to

be a standard practice to design these members by means of rough design rules for what regards LTB. Several research efforts have nevertheless been undertaken. In the early 80's, Nethercot (1982) and Kerdal (1984) conducted a series of experimental tests on castellated beams in bending, dedicated to the identification of specific failure modes. Years later, a European project entitled "Lateral Torsional Buckling in Steel & Composite Beams", (ECSC 2002) was partly devoted to cellular and castellated beams; however, this research project did not investigate the subject deep enough, providing a few tests results and no real design proposal. Additional information may be found in Radic (2008), El-Sawy (2009) and Sweedan (2011), where proposals for the determination of the critical bending moment M_{cr} in cellular and castellated beams are given; several topics relative to various other aspects of the behavior of castellated beams (distortion) are also treated in Zirakian (2006), Lakusic (2008), and Ellobody (2012). Other investigations related to instabilities of cellular or castellated beams may also be found in the literature, such as the flexural buckling behavior (Sweedan 2009, Verwij 2010), or beam-column behavior (Sonck 2010, 2011).

In 2004, a second RFCS project (ECSC 2004), "Large Web Openings for Service Integration in Composite Floors", was achieved, however more dedicated to isolated openings, thus not relevant for present investigations. One may also refer to experimental, numerical and analytical investigations performed at CTICM on cellular beams (Bitar 2006, Martin 2006); however, the specific LTB behavior was not addressed.

Considering all of this, it appears that no fully satisfactory design solution for the ultimate LTB resistance of cellular beams has been developed so far. Preliminary results also indicate that a high level of inaccuracy may be found in current practical solutions, potentially leading to highly uneconomical design. Present research developments aim at improving this situation through both experimental and numerical investigations. In this respect, Section 2 briefly depicts a series of three full-scale tests that have been performed at the College of Engineering and Architecture of Fribourg. Besides, FEM shell models have been derived, and, since showing a very good agreement with the tests (Section 3), they have been further used to gather a large set of GMNIA[5] reference results. Finally, Section 4 proposes new design formulae whose accuracy and adequacy is tested against the whole set of FEM reference results.

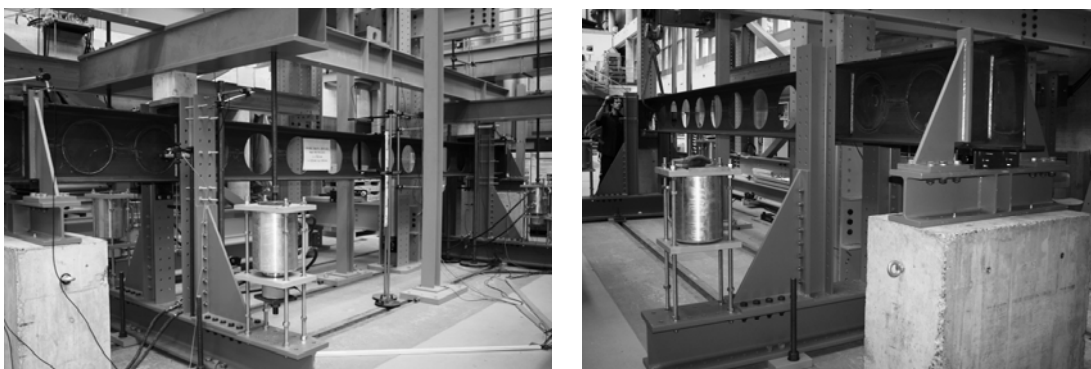## 2. Experimental activities

2.1 General test setup

Figure 3: a) General setup of LTB tests – b) Supports

---

[5] GMNIA: Geometrically and Materially Non-linear with Imperfection Analysis

3

A series of three LTB tests was performed at the Structural Engineering Laboratory of the College of Engineering and Architecture of Fribourg (see Fig. 3). These have consisted in "4-point" bending tests, on members spanning from 7.5 to 11 m. Accordingly, the middle segment of the girder is acted by a constant bending moment distribution (thus free form shear force), while the adjacent segments support linearly varying bending moments.
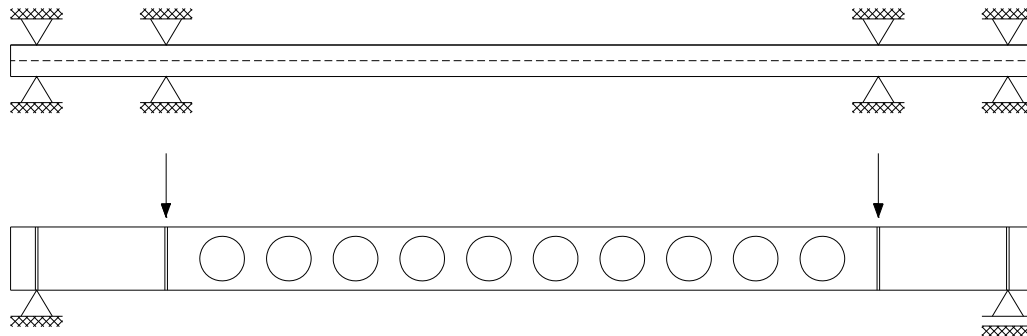

Figure 4: Principles of load application and support conditions (top and side views)

The supports arrangement was intended at offering vertical, lateral and torsional restraints as schematically represented on Fig. 4. As can be seen, the usual "reference situation" towards LTB (i.e. constant bending moment and fork conditions) is not strictly fulfilled for the middle part of the beam, since the end segments provide flexural (weak axis) and warping restraints. Further, the lateral supporting system may not be seen as providing i) an infinite lateral stiffness (separate measurement of this stiffness has however been performed), and ii) a strictly punctual lateral support. Within validation study of the FE-models, these aspects have been explicitly taken into account, as closely as what was done experimentally.
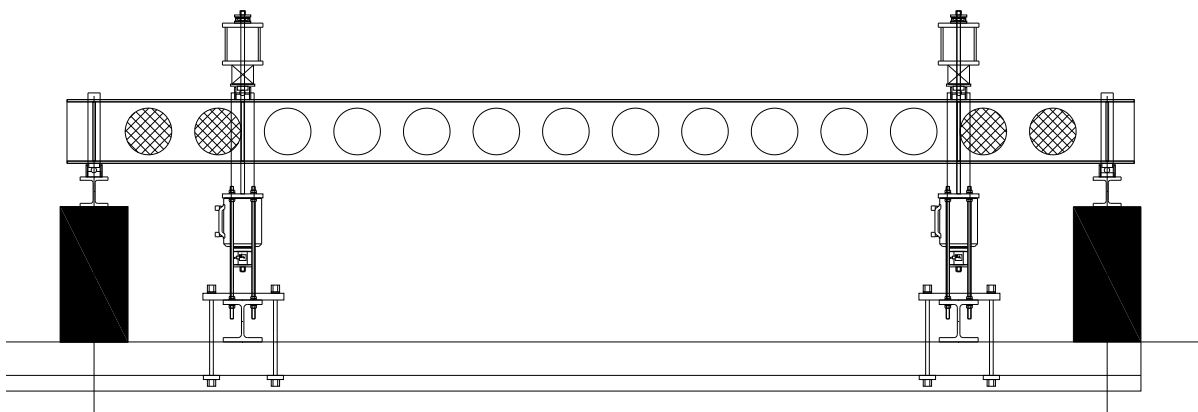

Figure 5: Practical test setup for loading and support conditions (side view)

As Figs. 3a, 5 and 6 show, loads have been applied through the use of four hydraulic jacks and by means of two rigid hollow girders placed above the top flange. The latter was also relying on a bloc of timber in order to ensure sufficient vertical displacement, which, in turn, was placed on a ruler support so that the applied loading on the top flange was almost punctual (see Fig. 6b). Loading was applied through usual displacement-controlled techniques up to failure.

Figure 6: Rigid girder and roller support for load introduction

In addition to the measurement of the applied load (by means of load cells), a series of displacements was measured continuously during each test, with a system of 22 LVDTs. Figs. 7a and 7b give an overview of the positioning and nature the various devices for the end and middle cross-sections, respectively.
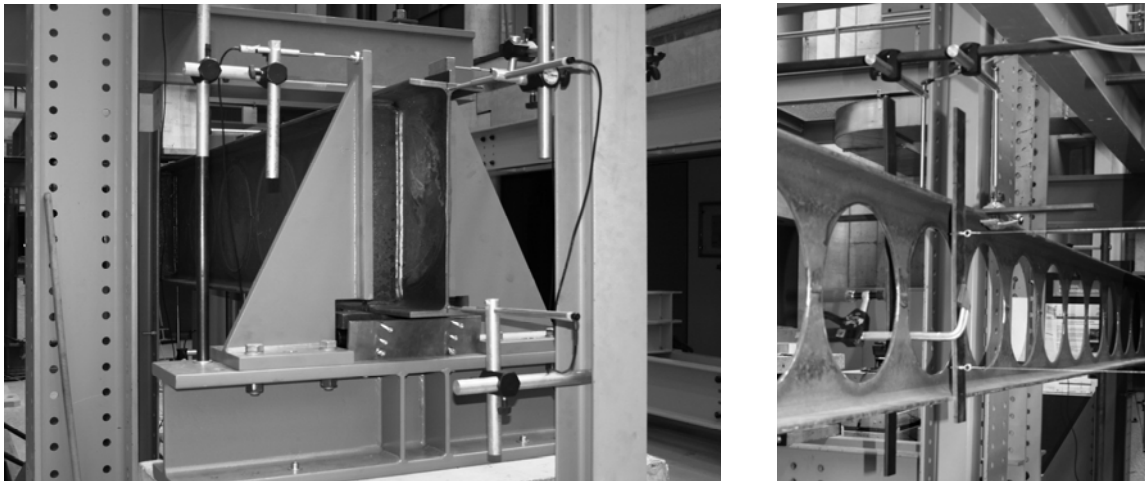

Figure 7: Instrumentation of a) End cross-section – b) Mid-span cross-section

No other type of measurement devices (rosettes, inclinometers…) has been used, since the information on the evolution of the displacements under load increase was sufficient to validate the FE-models. As a specific point, the mid-span cross-section was instrumented with a combination of four LVDTs, in order to capture information on i) the vertical *global*

displacement of the cross-section, on ii) the *global* lateral displacement and on iii) the torsional twist (Fig. 7b).

2.2 Material tests – Measurements of initial imperfections

In order to get accurate information on the real $\sigma - \varepsilon$ constitutive law, usual coupon tests have been performed. Two coupon specimens per member have then been tested, through a loading protocol that includes a partial unloading branch at 1% strain, so that to get an additional measurement of the Young's modulus E (see Fig. 8a). Following Table 1 reports on the accordingly-measured material properties. The obtained $\sigma - \varepsilon$ constitutive laws have also been introduced in the FEM models (see § 3.1), through multi-linear $\sigma - \varepsilon$ laws; use of linear regression analysis has been made to determine the various parameters needed, see Table 1.
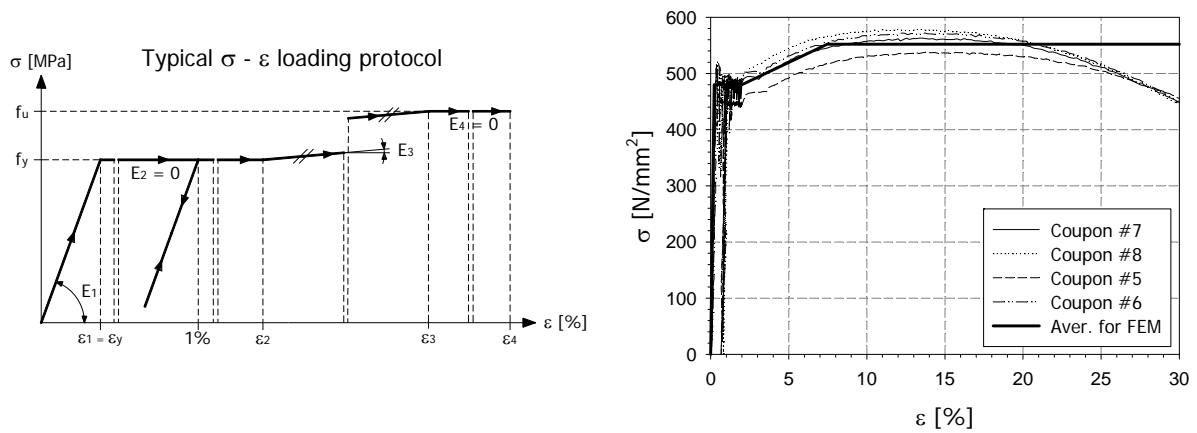

Figure 8: a) Typical loading protocol for coupon tests – b) Results for "HEA 340-based" coupons

Table 1: Results of the coupon tests

Coupon # (base profile)	1st slope			2nd slope	3rd slope			4th slope
	f_y [N/mm²]	ε_1 [%]	E_1 [GPa]	ε_2 [%]	f_u [MPa]	ε_3 [%]	E_3 [MPa]	ε_4 [%]
1 (Angelina)	285	0.17	173.7	1.98	407	6.93	2465	30
2 (Angelina)	283	0.19	148.9	1.98	393	6.98	2200	30
3 (Angelina)	284	0.18	157.8	2.00	393	6.99	2184	30
4 (Angelina)	290	0.20	145.0	2.00	407	7.03	2328	30
Average	*286*	*0.18*	*156.1*	*1.99*	*400*	*6.98*	*2294*	*30*
5 (HEA 340)	480	0.20	230.0	2.00	522	7.85	1060	30
6 (HEA 340)	488	0.25	195.2	2.00	565	7.98	1288	30
7 (HEA 340)	482	0.22	219.1	2.00	556	8.01	1231	30
8 (HEA 340)	490	0.24	204.2	2.00	564	6.00	1850	30
Average	*480*	*0.23*	*212.1*	*2.00*	*552*	*7.46*	*1357*	*30*
9 (IPE 330)	373	0.21	177.6	2.00	481	5.03	3564	30
10 (IPE 330)	372	0.22	169.1	2.00	480	5.10	3484	25
Average	*373*	*0.22*	*173.4*	*2.00*	*481*	*5.07*	*3524*	*28*

1. Δ_{lat} stands for initial (lateral) imperfection, and ψ_{ini} for the initial torsional twist

Besides the determination of the material characteristics, measurements of the actual dimensions of the cross-section have been performed; results are reported in Table 2. As Fig. 9 shows, it may be noted that a non-negligible "bending of web" default was measured (about 5° slope compared to a horizontal plane).

Table 2: Measured cross-sectional geometrical characteristics

Base profile	h_{left} [mm]	h_{right} [mm]	b_{up} [mm]	b_{lo} [mm]	$t_{f,up}$ [mm]	$t_{f,lo}$ [mm]	$t_{w,up}$ [mm]	$t_{w,lo}$ [mm]
Angelina	518.6	517.9	160.8	160.2	11.9	11.9	8.1	8.1
HEA 340	465.8	472.1	297.1	297.7	16.0	16.0	10.4	10.3
IPE 330	446.0	446.5	161.4	161.7	10.8	10.7	7.9	7.6

Figure 9: "Bending of web" initial cross-sectional imperfection

Further, an original method for the measurement of the initial geometrical imperfections has been specifically developed. A combination of three different improved topometric techniques has been used to provide a three-dimensional representation of the beam, providing an overall level of accuracy of all the measured initial imperfections that is estimated to be around ±0.3 mm.
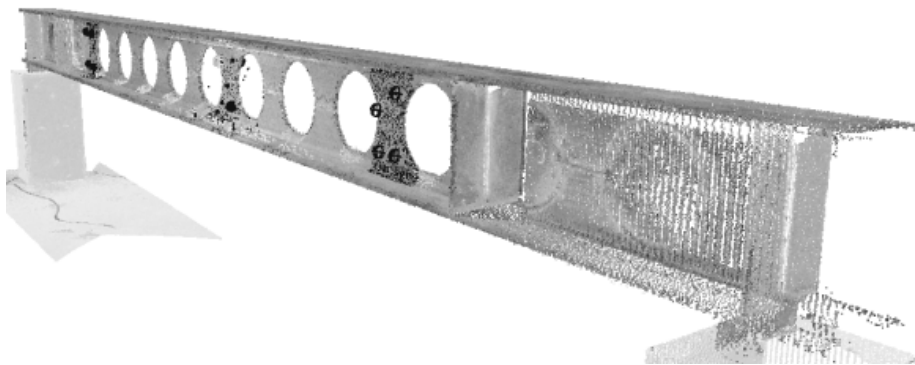

Figure 10: Global scan of a girder

The first technique has consisted in a global scanning of each member, by means of a dedicated theodolite. Featuring more than 100 000 measured targets, a global "cloud of targets" of the beam has been established, with an accuracy of ± 3 mm (see Fig. 10).

Second, a purposely-developed optical system has been employed for an accurate 3D representation of the flanges' edges. These measurements have basically consisted in measuring accurately (± 0.2 mm accuracy) the position of a "light source" (in practice, a diode) placed upon the flange's edge, over a longitudinally-moving trolley. Typical "measurement steps" of 50 mm have used to describe all of the four edges, for each girder.

Figure 11: Measurement of flanges' edges a) Trolley and light – b) optical measure

Finally, refined scans of some local areas on the member (200 x 100 mm) have been made, with an accuracy of ± 0.2 mm. Both external surfaces of the web have been measured, and, after numerical treatment, an average surface has been kept for introduction in the FE models.
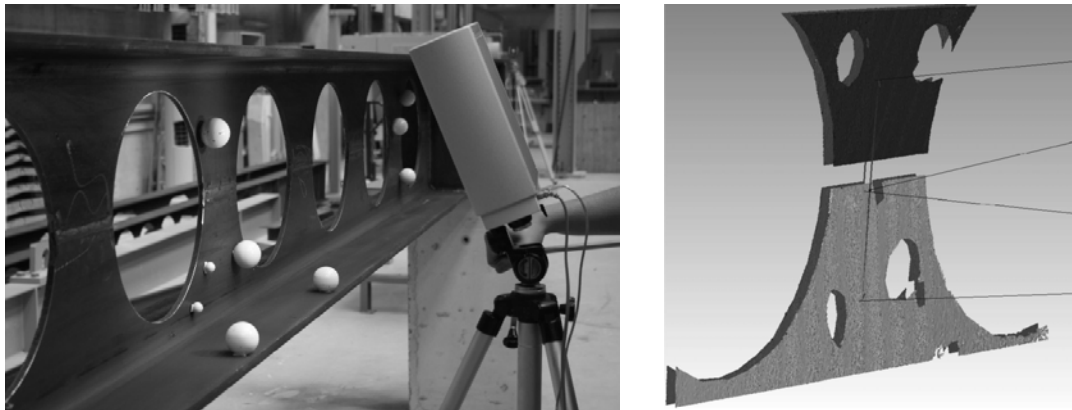

Figure 12: a) Local scanning of web imperfections – b) Geometry after numerical treatment

Sophisticated and rigorous treatments of the measurements, together with interpolation techniques using the data from all three systems, have made possible the accurate and realistic definition of an initial imperfect geometry of the FE mesh, where all nodes bear initial imperfections. Figs. 13a and 13b propose a magnified view of the obtained "imperfect" mesh in the central part of the girder.
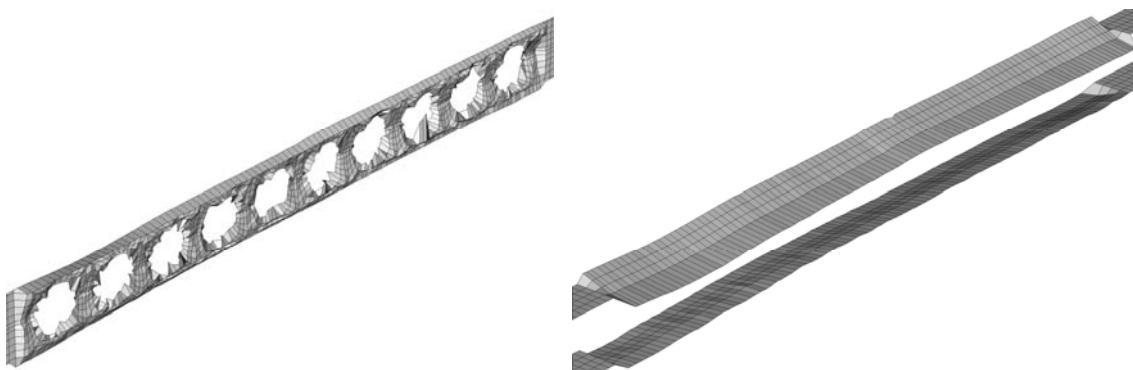

Figure 13: Amplified deformed patterns for the web and flanges (Magnified 20 times, base profile: HEA 340)

Finally, one may specify that neither measurements nor investigations towards the determination of residual stresses have been undertaken. This is motivated by the fact that i) the state of residual stresses in such girders is highly complex, since it results from a series of industrial processes having important effects on the distribution of residual stresses (base profile hot-rolling, flame cutting, final re-welding)[6], and ii) because it is of standard practice to locally apply important flame heating in the regions of the web that may lie outside the fabrication tolerances; these unpredictable operations definitely ruin the possibility to scientifically predict the state of residual stresses in such members.

2.3 Member test results

Table 3 summarizes the measured loads and displacements recorded at failure. Figs. 15a and 15b also reflect the behavior observed during the tests.

Table 3: Results for LTB experimental tests

Base profile	P_{max} [kN]	$\Delta_{vert.\ max}$ [mm]	$\Delta_{lat.\ max}$ [mm]	ψ_{max}[1] [rad]	s[2] [mm]	a_0 [mm]
Angelina	235.1	59.4	6.35	0.015	1100	380
HEA 340	1977	74.7	15.6	0.035	515	345
IPE 330	176.9	62.3	24.5	0.075	395	345

1. ψ_{max} stands for the measured torsional twist, and P_{max} represents the total vertical load applied on the member
2. s and a_0 denote geometrical characteristics which are typical of cellular members
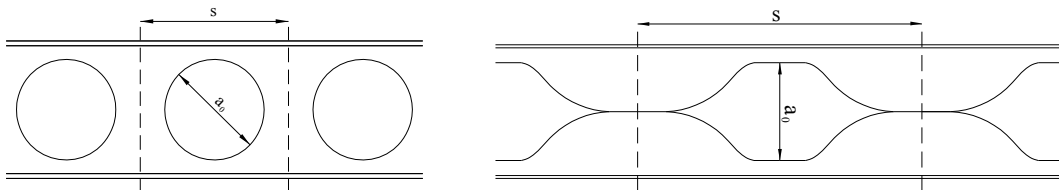

Figure 14: Geometrical description of tested elements a) Cellular type – b)Angelina type

Figure 15: a) Lateral torsional deformed configuration at failure – b) Residual deformation after unloading

---

[6] One may also take due account of the sequence of all operations

3. Numerical developments

3.1 Development and assessment of FEM models

Extensive series of numerical computations have been led with the use of non-linear FEM software FINELg, continuously developed at the University of Liège and Greisch Engineering Office since 1970. This software offers almost all types of FEM types of analyses, and present investigations have mainly been resorting to so-called MNA (Materially Non-linear Analysis), LBA (Local Buckling Analysis) and GMNIA analyses. Use of quadrangular 4-nodes plate-shell finite elements with typical features (Corotational Total Lagrangian formulation, Kirchhoff's theory for bending) has been made. Density and quality of the different meshes used here has been preliminarily assessed, and, in a first step, FE modeling of the different experimental configurations has been done. They have been built with all preliminary measured data, namely the geometry and dimensions of the girders, the measured thicknesses, $\sigma - \varepsilon$ constitutive laws and initial geometrical imperfections. The following Table 4 proposes the results of the comparison between experimental and numerical results.
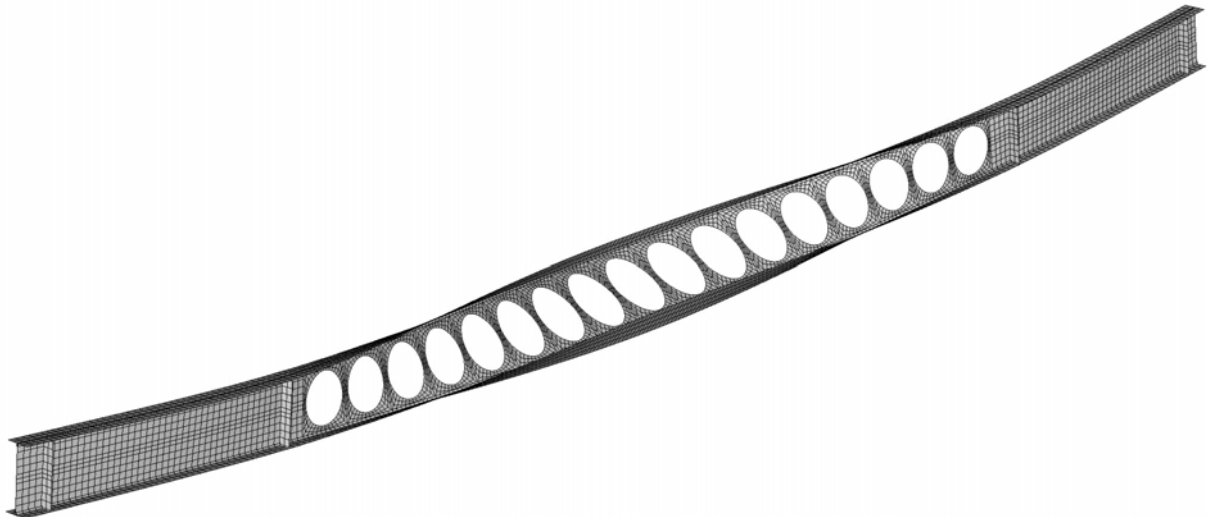

Figure 16: FE deformed configuration at failure – Base profile: IPE 330 (amplification factor: 5)

Table 4: Comparison between experimental tests and FEM results (at max. load)

Base profile		P_{max} [kN]	$\Delta_{vert.\,max}$ [mm]	$\Delta_{lat.\,max}$ [mm]	ψ_{max} [rad]
Angelina	Test	235.1	59.4	6.35	0.86
	FEM	182.1	60.2	23.5	4.01
	Ratio	0.77	1.01	3.7	4.61
HEA 340	Test	1977	74.7	15.6	1.88
	FEM	2071	69.3	1.79	0.57
	Ratio	1.05	0.93	0.11	0.28
IPE 330	Test	235.1	62.3	24.5	4.52
	FEM	164.7	73.1	37.3	8.02
	Ratio	0.93	1.17	1.52	1.84

Figs 17a and 17b also compare the FEM-experimental load – displacement behavior of some specimens.
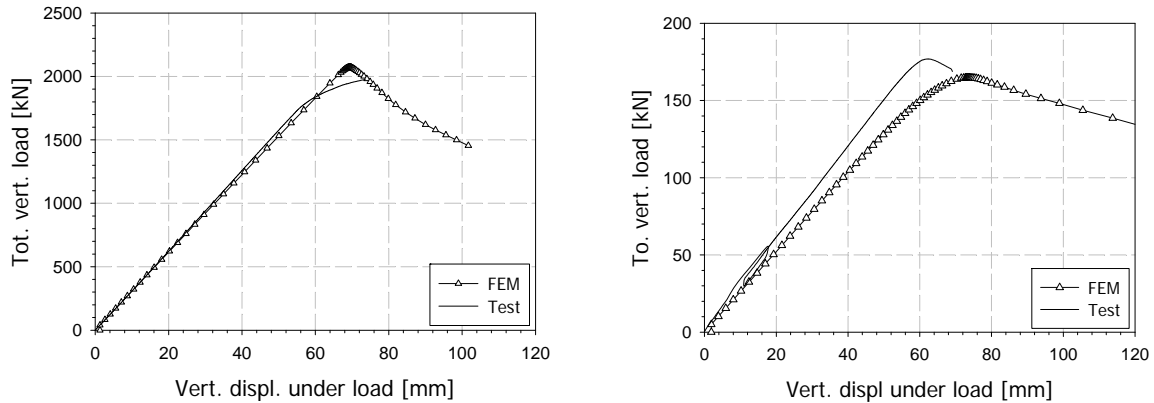
Figure 17: Load-displacement behavior a) Base profile: HEA 340 – b) Base profile: IPE 330

As Table 4, Figs. 17a and 17b show, excellent agreement between the tests and the FEM models is observed. Detailed analysis and comparison of both sources of results also demonstrates that the FEM models are able to provide reliable results (i.e. ultimate loads) and may be safely "substituted" to experimental tests.

3.2 Parametric studies

The developed FE-models being shown to be adequate, they have been extensively used within parametric studies that aim at collecting reference results in order to validate/invalidate a simplified design proposal. The various parameters accounted for in these parametric studies have been chosen so as to represent closely the whole set of potential practical applications. Further, production, erection and service constraints have been taken into account.

Accordingly, the following set of parameters has been retained in the numerical studies:

- 6 cross-sections: IPE 300, IPE 400, IPE 600, HEA 400, HEB 800, HEM 1000;
- 5 bending moment distributions, respectively load cases 1 to 5: constant ($\beta^7 = 1.0$), linear ($\beta = 0.5$ and $\beta = 0$), uniformly distributed transverse load (applied on top flange), and Concentrated load at mid-span (top flange);
- 4 values of parameters s (relative size of the openings, see Fig. 14): $s = 1.12\,a_0$, $s = 1.25\,a_0$, $s = 1.50\,a_0$, $s = 1.75\,a_0$;
- 2 different steel grades: S235 and S460;
- 8 different values of λ_{LT} for each $\chi_{LT} - \lambda_{LT}$ single curve (see § 4.2).

It is to be mentioned that typical "fork conditions" have been used in the modeling, as well as the following generic initial imperfections (more details of the FE modeling are given in Boissonnade 2012):

- No residual stresses;
- Local imperfections defined as square half-wave patterns in both directions of the considered plates, with an amplitude of $a\,/\,400$, where a stands for the length of the considered "square" panel;

---

[7] β stands for the end-moments ratio ($-1 \leq \beta \leq 1$)

- Global imperfections, set as the combination of a lateral sinusoidal imperfection with amplitude $L / 500$[8], and of an initial torsional twist with maximum amplitude at mid-span equal to $L / (2000\ H)$.

Critical and ultimate calculations have been made for all cases, so that in total nearly 4 000 FE-shell non-linear simulations have been performed; these "reference results" have been further used for the assessment of the proposed design rules, see § 4.2.

4. Proposal for new design rules

4.1 Improved design rules

As explained in the introduction, the actual design rules provided by ArcelorMittal (ACB+, 2010) can be shown to be far too conservative (see also next paragraph). They basically consist in considering the sole buckling resistance of the upper "Tee" of the weakest cross-section. This reduced cross-section is considered as acted by compression forces only, and is therefore verified against flexural lateral buckling, with a buckling length set equal to the length between points of lateral support.

Even if the actual bending moment distribution on the member is taken into account by means of a variable level of axial compression in the Tee, this design proposal leads to very conservative estimates of the LTB resistance, mainly because:

- The stabilizing effect of the flange in tension is fully neglected;
- The torsional stiffness of the whole cross-section is also disregarded;
- Considering the Tee of the weakest cross-section neglects the beneficial material in between consecutive holes; this, in many cases (e.g. typical "floor" beams), may have an important influence.

In order to significantly improve these design rules, the following design procedure is proposed:

- Determine the section properties of the weakest cross-section: $M_{y,Rk}$, I_z, I_t, I_ω;
- Calculate the critical bending moment, on the basis of these properties (by means of usual approximate formulae, see ECSC 2002 for example);
- Calculate $\lambda_{LT} = (M_{y,Rk} / M_{cr})^{0.5}$;
- Determine the "reduction factor" due to LTB χ_{LT} with the use of buckling curve "c" (see Eurocode 3, 2005);
- Calculate $\chi_{LT,\mathrm{mod}}$[9];
- Finally, the ultimate bending moment $M_{ult,y,Rd} = \chi_{LT,\mathrm{mod}} \cdot M_{y,Rd}$, where $M_{y,Rd}$ further accounts for the usual safety factor γ_M.

This design procedure closely follows the actual European LTB design rules for standard rolled and welded beams, except i) for what concerns the use of the weakest cross-section and ii) the use of buckling curve "c" for all situations.

---

[8] This value, higher than usually adopted ones, is intended at indirectly covering the influence of residual stresses

[9] $\chi_{LT,\mathrm{mod}}$ accounts for potential beneficial effects due to a non-constant distribution of the bending moment along the member, see Eurocode 3, 2005;

4.2 Validation against FEM results

Figs. 18a and 18b first illustrate the improved accuracy brought by the proposed design procedure, in comparison with the actual "ACB+" rules. An increasing level of over-conservatism of the ACB+ prediction can also be pointed out, when the number of holes (i.e. the slenderness) of the member increases. As Fig. 18b shows, the ratio $\chi_{LT, FEM} / \chi_{LT, ACB+}$ can reach values up to 2.5, meaning that the ACB+ provisions may be extremely conservative, for girders' geometries which still remain close to practical applications. Identical conclusions have been found for almost all cases, confirming i) the need for improved rules and ii) the excellent level of accuracy of the new design proposal.
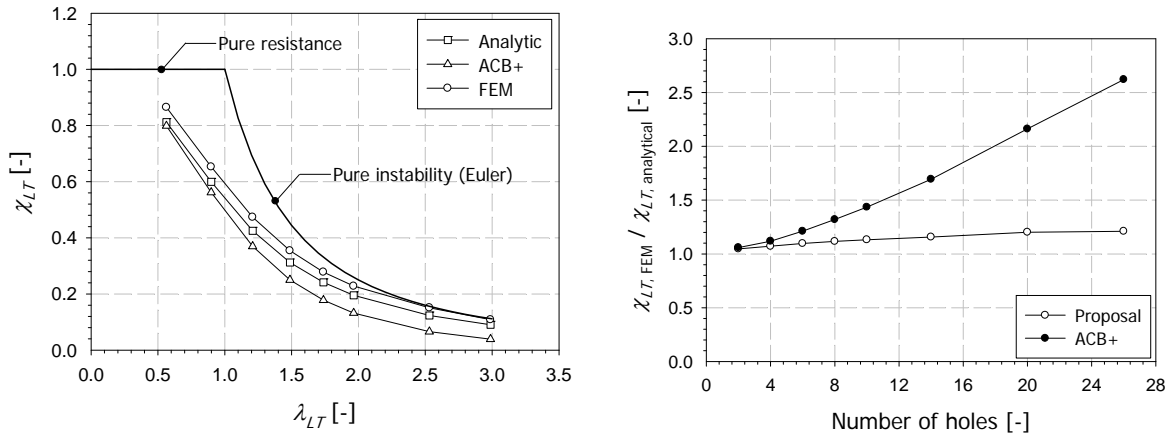

Figure 18: Results for base profile IPE 600, load case 1 (constant bending moment), $s = 1.75\ a_0$, S460

As a further illustration of the observed tendencies, Table 5 proposes statistical results of the comparison between FEM, ACB+ and "proposal" results in the particular case of an IPE 600 base profile, steel grade S460. As can be seen, the resistance estimates are significantly improved by the new proposal, and the mean and standard deviation values also indicate a high level of consistency. This is further illustrated by the histograms of Figs. 20a, 20b, 21a and 21b, where the comparisons between histograms clearly demonstrate the improved accuracy features of the proposed new rules. A detailed analysis of all available results of the parametric FEM study confirms the observed trends, whatever the set of parameters. The proposed design rules are then seen to be much more accurate than the actual ones, potentially leading to significant material savings.

Table 5: Comparison between FEM, ACB+ and proposal results (base profile IPE600, S460)

	Nb of FEM results	$\chi_{LT, FEM} / \chi_{LT, proposal}$				$\chi_{LT, FEM} / \chi_{LT, ACB+}$			
		Min[1]	Max	Average	St. dev	Min	Max	Average	St. dev
Load case 1	40	1.05	1.22	1.13	0.05	1.05	2.71	1.56	0.52
Load case 2	40	0.82	1.71	1.27	0.21	1.05	3.37	2.17	0.62
Load case 3	40	0.40	1.83	1.24	0.33	0.44	2.89	1.72	0.65
Load case 4	40	0.32	1.68	1.12	0.37	0.31	2.15	1.16	0.53
Load case 5	40	0.41	2.17	1.31	0.46	0.41	2.49	1.27	0.56
$s = 1.12\ a_0$	45	0.32	1.81	1.11	0.36	0.31	2.9	1.38	0.67
$s = 1.25\ a_0$	45	0.40	1.99	1.21	0.33	0.39	2.69	1.50	0.60
$s = 1.5\ a_0$	45	0.39	1.79	1.20	0.26	0.37	3.37	1.61	0.69
$s = 1.75\ a_0$	45	0.57	2.17	1.33	0.29	0.54	3.34	1.82	0.67

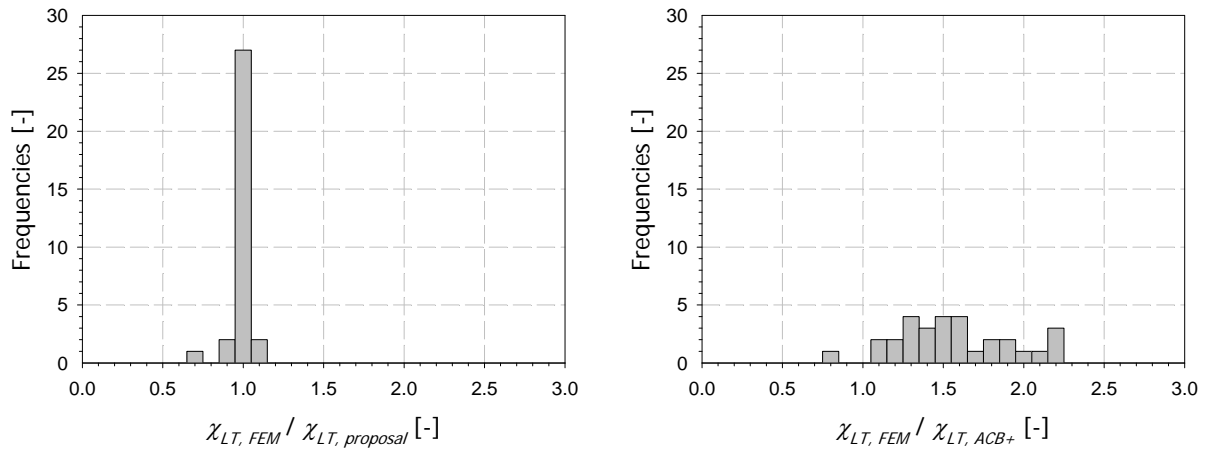1. Very low values should be disregarded since the observed failure modes differ from LTB

Figure 20: Frequency distribution of the ratio $\chi_{LT, FEM}$ / $\chi_{LT, analytic}$ for an HEB 800, S460, load case 2, all sizes of openings – a) Proposal – b) ACB+
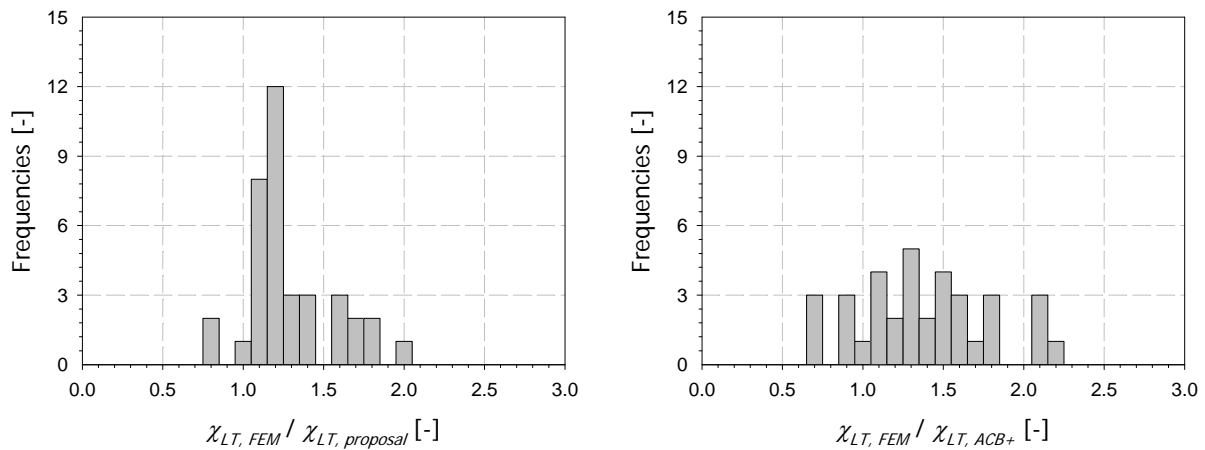

Figure 21: Frequency distribution of the ratio $\chi_{LT, FEM}$ / $\chi_{LT, analytic}$ for an IPE 600, S235, all load cases, $s = 1.25\ a_0$ a) Proposal – b) ACB+

5. Conclusions – Future developments

This paper investigates the LTB resistance of so-called "cellular" steel beams, through both experimental, numerical and analytical (design) aspects. A series of three full-scale tests is first reported, whose main purpose was the validation of purposely-developed FE-models. Since showing an excellent agreement with the experimental results, they have been further used in extensive parametric studies. In total, nearly 4 000 FEM "reference" results have been gathered, covering the various influences of cross-sectional shape, bending moment distribution, relative size of the openings, and yield stress. They have later served as a database of reference results for the validation of an original design proposal.

A proposal for improved design rules is also detailed; in comparison with all available FEM results, they are shown i) to substantially improve the global accuracy of the design procedure (thus allowing for significant material savings), and ii) to provide safe and reasonably accurate estimates of the "real" LTB resistance of such girders. Accordingly, the design proposal may be recommended for practical design as well as for design code implementation.

14

Finally, one should mention that research developments towards the behavior of cellular members under combined bending and compression are actually under way, in order to offer the possibility to resort to structural solutions involving cellular members used as columns or beam-columns.

Acknowledgments

References

ACB+ (2010). ArcelorMittal Cellular Beams software ACB+ v2.02, Long Carbon Europe Research Centre.

Angelina (209). Angelina software v1.01, ArcelorMittal Commercial Sections.

Bitar, D., Martin, P.O., Galéa, Y., Demarco, T. (2006). "Poutres cellulaires acier et mixtes : partie 1 proposition d'un modèle pour la résistance des montants". *Construction Métallique n°1.*

Boissonnade, N., Somja, H. (2012). "Influence of Imperfections in FEM Modeling of Lateral Torsional Buckling". *Proceedings of the Annual Stability Conference, Structural Stability Research Council, Grapevine, Texas, April 18-21.*

ECSC (2002). "Lateral torsional buckling in steel & composite beams", *project n° ECSC 7210-PR-183.*

ECSC (2004). "Large Web Openings for Service Integration in Composite Floors", Project n°7210-PR-315.

Ellobody, E. (2012). "Interaction of buckling modes in castellated steel beams". *To be published in Journal of Constructional Steel Research.*

El-Sawy, K, Sweedan, A., Martini, M. (2009). "Major-axis elastic buckling of axially loaded castellated steel columns". *Thin-Walled, Structures, 47, pp. 1295–1304.*

Kerdal, D., Nethercot, D. (1984). "Failure Modes for Castellated Beams". *Journal of Constructional Steel Research, 4, pp. 295–315.*

Lakusic, V. T., Dzeba, I., Androic, B. (2008). "The buckling curve for lateral-torsional buckling resistance of castellated beams". *Proceedings of the 5th European Conference on Steel Structures, Eurosteel 2008, Graz, pp. 1587-1592, September 3-5.*

Martin, P.O., Galéa, Y., Bitar, D., Demarco, T. (2006). "Poutres cellulaires acier et mixtes : partie 2 proposition de nouveaux modèles analytiques de calcul de la fleche". *Construction Métallique n°2.*

Nethercot, D., Kerdal, D. (1982). "Lateral-torsional buckling of castellated beams". *The Structural Engineer, 60b, pp. 53–61.*

Radic, I., Markulak, D., Veravac, D. (2008). "Numerical simulation of lateral stability of castellated beams". *Proceedings of the 5th European Conference on Steel Structures, Eurosteel 2008, Graz, pp. 1593-1598, September 3-5.*

Sonck, D., Vanlaere, R., Van Impe, R. (2010). "Elastic buckling of cellular members loaded by an axial force". *Proceedings of the International Association for Shell and Spatial Structures (IASS) Symposium 2010, Shanghai.*

Sonck, D., Van Impe, R. (2011). "Elastic Buckling of Cellular Members Loaded by an Eccentric Axial Force". *Proceedings of the 6th European Conference on Steel Structures, Eurosteel 2011, Budapest, August 31 - September 2.*

Verwij, J. (2010). "Cellular beam-columns in portal frame structures". *Master thesis, T.U. Delft.*

Sweedan, A. (2011). "Elastic lateral stability of I-shaped cellular steel beams". *Journal of Constructional Steel Research, 67, pp 151–163.*

Zirakian, T., Showkati, H. (2006). "Distortional buckling of castellated beams". *Journal of Constructional Steel Research, 62, pp. 863–871.*